Chinese Chemical Letters 34 (2023) 107528

Contents lists available at ScienceDirect

Chinese Chemical Letters

journal homepage: www.elsevier.com/locate/cclet

Integration exosomes with MOF-modified multifunctional scaffold for accelerating vascularized bone regeneration

Chang Xu[a], Yue Kang[b], Xufeng Dong[a,*], Daqing Jiang[b], Min Qi[a,*]

[a] School of Materials Science and Engineering, Dalian University of Technology, Dalian 116024, China
[b] Department of Breast Surgery, Cancer Hospital of China Medical University, Shenyang 110042, China

ARTICLE INFO

Article history:
Received 28 February 2022
Revised 11 May 2022
Accepted 11 May 2022
Available online 16 May 2022

Keywords:
Exosomes
Osteogenesis
Angiogenesis
Metal-organic framework
Bone regeneration

ABSTRACT

Designing a multifunctional scaffold with osteogenic and angiogenic properties holds promise for ideal bone regeneration. Innovative scaffold was here constructed by immobilizing exosomes derived from human bone mesenchymal stem cells (hBMSCs) onto porous polymer meshes which developed by PLGA and Cu-based MOF (PLGA/CuBDC@Exo). The synthesized exosome-laden scaffold capable of providing a dual cooperative controllable release of bioactive copper ions and exosomes that promote osteogenesis and angiogenesis, thereby achieving cell-free bone regeneration. *In vitro* assay revealed the composite stent not only substantially upregulated the expression of osteogenic-related proteins (ALP, Runx2, Ocn) and VEGF in hBMSCs, but promoted the migration and tube formation of the human umbilical vein endothelial cells (HUVECs). *In vivo* evaluation further confirmed this scaffold dramatically stimulated bone regeneration and angiogenesis in critical-sized defects in rats. Altogether, this composite scaffold carrying therapeutic exosomes had an osteogenic-angiogenic coupling effect and offered a new idea for cell-free bone tissue engineering.

The repair and treatment of bone defects has always been a huge challenge for clinicians [1–4]. However, bone tissue repair involves a cascade of complex steps, including osteogenesis, angiogenesis and inflammation, in this regard, osteogenesis and angiogenesis are tightly coupling to each other [5–7]. Blood vessels often play an important role in the process of ossification and bone reconstruction due to they can supply nutrients [8–10]. However, early angiogenesis after implantation of bone grafts is limited, which severely delay bone tissue healing [11]. Definitely, dual-functional regulation of osteogenesis and angiogenesis is necessary for successful bone regeneration [12].

Latest researchers have found that the exosomes secreted by mesenchymal stem cells (MSCs) hold promise for tissue regeneration [13,14]. Exosomes are extracellular vesicles with a diameter of 40–160 nm and contain a variety of bioactive molecules, which have similar biological effects to their derived cells [15]. More specifically, the exosomes can promote osteogenesis and angiogenesis in the absence of MSCs, and much easier to prepare, handle, characterize and store [16–18]. However, due to its defects such as rapid degradation *in vivo* and relatively short half-life, most injected exosomes accumulate less in the focus region, which seriously influences their effect [19]. In addition, the biological efficacy of exosomes can hardly maintain due to the process of bone regeneration is usually long-term and complex [20]. Hence, it is highly desirable to develop a biocompatible scaffold with the flexible and stable immobilizing of exosomes to exert therapeutic roles for bone tissue repair.

Using bioengineered scaffolds with porous or lattice structure are vital in bone regeneration [21–23]. Metal-organic framework (MOF) is a class of porous framework material composed of metal ions or clusters with organic ligands, due to its structural diversity and large surface area, has been commonly used in biological applications [24–26]. Copper-based MOFs benefit from the multifunctionality of Cu^{2+}, which exhibit antibacterial, osteogenic, pro-angiogenic and antioxidant effects, also occupy a vital position in the field of biomaterial [27–30]. As a type of bioactive ion, Cu^{2+} promotes osteogenesis by inducing early osteoblast differentiation of MSCs and initiating an appropriate immune microenvironment, so Cu^{2+} ions are a highly anticipated option for bone tissue engineering [31].

On these bases, an innovative scaffold was fabricated here by incorporating copper-based MOF [copper 1,4-benzenedicarboxylate (CuBDC)] with poly(lactic acid-*co*-glycolic acid) (PLGA), and thus, immobilizing exosomes derived from human bone mesenchymal stem cells (hBMSCs-Exo) onto the fibrous polymer meshes for ac-

* Corresponding authors.
E-mail addresses: dongxf@dlut.edu.cn (X. Dong), minqi@dlut.edu.cn (M. Qi).

https://doi.org/10.1016/j.cclet.2022.05.042
1001-8417/

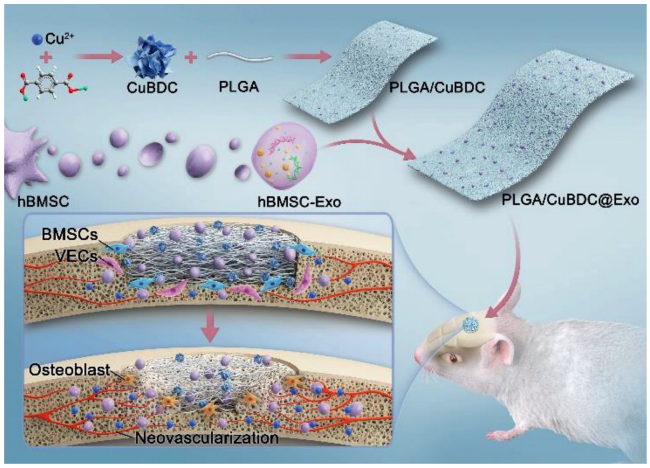

Scheme 1. Schematic illustration of exosome-laden PLGA/CuBDC scaffold (PLGA/CuBDC@Exo) for the repair of bone defects. The well-designed scaffold was implanted into rat calvarial defect mode to evaluate the osteogenic ability of BMSCs and pro-angiogenic ability of vascular endolial cells (VECs).

celerating vascularized bone regeneration (Scheme 1). First, CuBDC was synthesized through a one-step process and organic solvent-freely. Subsequently, CuBDC were embedded into PLGA fibers through an electrospinning process. Finally, for the first time, exosomes were fixed on composite scaffold (PLGA/CuBDC@Exo), allowing this exosome-laden scaffold with unique nanostructure to achieve a dual cooperative controllable release of bioactive ions while also exerting the therapeutic effect of exosomes, thus enabling cell-free bone regeneration. The biocompatibility and osteogenesis-angiogenesis coupling effects of scaffold were investigated *in vitro*, and a well-established bone defect model was adopted to evaluate the bone repair effect *in vivo*. This rationally engineered strategy may be effective in achieving vascularized osteogenesis and providing new insight of designing cell-free based fibrous scaffolds.

The physical and biological features of the exosomes were evaluated. According to the observations of TEM image (Fig. 1a), it showed that the exosomes appear as spherical shapes with a diameter of 50–130 nm and had a bilayer membrane structure. Besides, the size and distribution of exosomes was performed by nanoparticle tracking analysis (NTA), the main peak value was located at 113.5 ± 1.3 nm ($n = 3$) (Fig. S1 in Supporting information). And the zeta potential was -31.4 ± 1.7 mV (Fig. S2 in Supporting information). Simultaneously, the results of western blotting confirmed that the extracted exosomes express three specific markers, CD9, CD81 and TSG101 (Fig. 1b). All these results solidly demonstrated the successful extraction of hBMSCs-Exo.

The CuBDC was synthesized through a facile method at room temperature and organic solvent-freely, the process was illustrated in Scheme 1. Notably, the PXRD pattern was used to reveal the structure of CuBDC crystal and present in Fig. 1c. This behavior was consistent with reported previously (P4 symmetry, $a = c = 11.19$, $b = 5.8$) [32,33]. Furthermore, it could be clearly seen from the scanning electron microscopy (SEM) image that the well-prepared CuBDC had a shape of nanoflower (Fig. 1c). It is worth mentioning that this unique morphology has certain active sites as well as a large specific surface area, allowing for a certain adhesion property. Moreover, the CuBDC exhibited nearly unchanged particle size during 24 h after incubation in PBS solution, displaying excellent stability (Fig. S3 in Supporting information). It has been well documented that PLGA fibrous meshes were prominent matrix for bone tissue engineering [34–37], and thus, the CuBDC were embedded into PLGA fibers through an electrospinning process. The

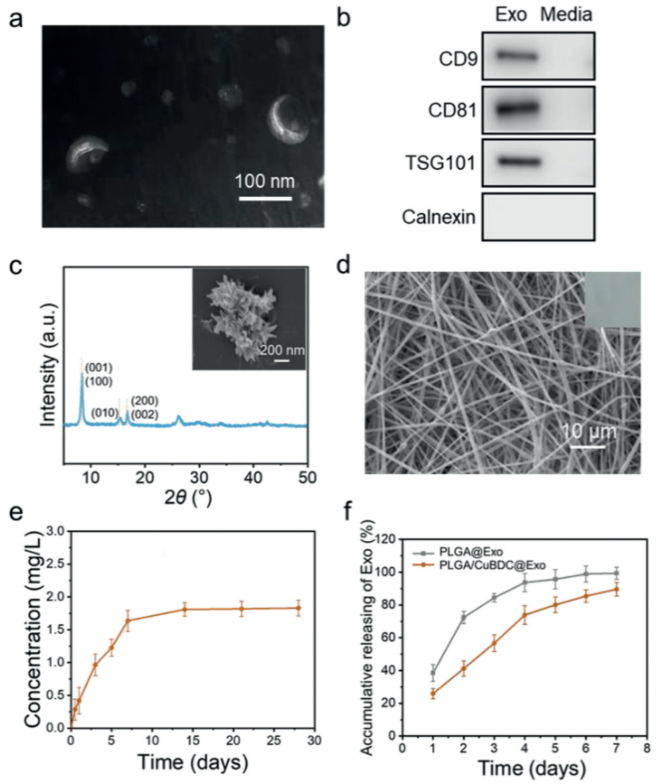

Fig. 1. Characterization of PLGA/CuBDC@Exo scaffold. (a) The morphology of hBMSCs-Exo was detected by TEM. (b) The specific marker proteins of CD9, CD81 and TSG101 were detected by Western blot. (c) PXRD pattern and SEM image of CuBDC. (d) Digital photos and SEM image of PLGA/CuBDC scaffold. (e) Cumulative release curve of copper ions in 28 days. (f) *In vitro* release curves of exosomes from PLGA and PLGA/CuBDC scaffolds.

digital photo and surface morphologies of the as-prepared scaffold were presented in Fig. 1d. The composite mesh was nonwoven membrane from macroscopical level, and long fibers that were randomly arranged and intertwined with each other at the microcosmic level. The FTIR was operated to identify the molecular structures and the results were shown in Fig. S4 (Supporting information). For CuBDC, the stretching vibration peaks of the benzene ring were located at 1502, 733 and 570 cm^{-1}, respectively. And the absorption peaks at 1587 and 1401 cm^{-1} were derived from stretching vibrations of carbonyl group. The main characteristic absorption peaks of PLGA appeared at 1183, 1083 and 1271 cm^{-1} corresponding to the C-O-C symmetric stretching vibration of ester bond, while 1753 cm^{-1} was assigned to the stretching vibration peak of C=O. For CuBDC-blended PLGA scaffold all possessed the absorption peaks of the carbonyl group and benzene ring from PLGA and CuBDC. Moreover, the XRD profiles further revealed that PLGA and CuBDC maintain their microstructure after electrospinning process (Fig. S5 in Supporting information). Surprisingly, the thermal stability of PLGA was significantly improved after the addition of CuBDC (Fig. S6 in Supporting information). Strikingly, the release kinetics of copper ions from the scaffold were monitored by ICP-AES (Fig. 1e). The MOF-modified scaffold could maintain a sustained and steady release of therapeutic copper ions without a burst-release more than 20 days, and thus, achieving a microenvironment with a certain amount of copper ion supply for cell growth. In addition, the stent could be slowly degraded and absorbed (Fig. S7a in Supporting information), with 75% of the mass remaining after 10 weeks (Fig. S7b in Supporting information), which fully meet the needs of biocompatible tissue engineering scaffold.

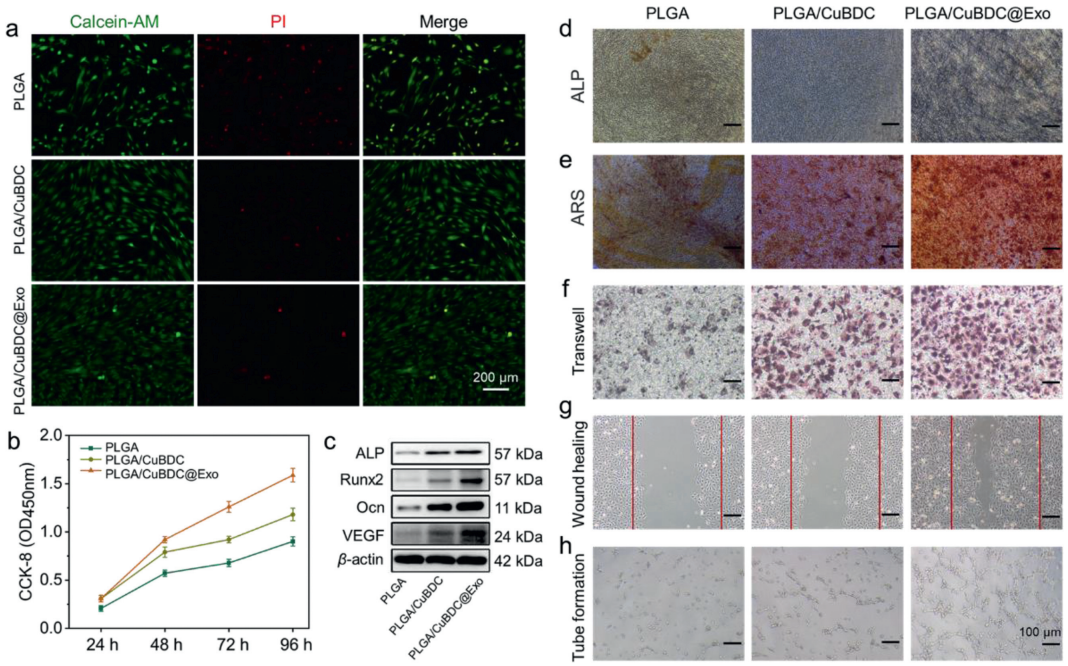

Fig. 2. The biocompatibility, osteogenic and pro-angiogenic effect of PLGA/CuBDC@Exo scaffold *in vitro*. (a) Live/dead staining of hBMSCs cultured on PLGA/CuBDC@Exo scaffold for 3 days. (b) CCK-8 assay of hBMSCs on scaffold. (c) Osteogenic and angiogenic-related protein expression in hBMSCs on scaffold by western blot. (d) ALP and (e) ARS staining of in the extracts of PLGA/CuBDC@Exo scaffold. Representative images of (f) Transwell assay, (g) wound healing assay and (h) tube formation assay for PLGA/CuBDC@Exo scaffold.

After co-incubation, exosomes were tethered to scaffold by physical embedding and electrostatic interactions, SEM images were shown in Fig. S8 (Supporting information), the surface of PLGA/CuBDC@Exo mat became rough and had nanoscale exosome-shaped particles. And to further visualize the distribution of exosomes on scaffold, the hBMSCs-Exo were labeled by Dil, it was clear that exosomes were evenly distributed on the scaffold compared to PLGA/CuBDC scaffold (Fig. S9 in Supporting information). Afterwards, the release kinetics of exosomes were assessed and shown in Fig. 1f. Compared to PLGA scaffold, PLGA/CuBDC enabled releasing of exosomes slowly, and nearly 11.4% of exosomes remained on the scaffold after 7 days. These results indicated that the introduction of CuBDC was an effective way for immobilized and sustained release of exosomes.

The viability and proliferation of hBMSCs on fibrous scaffolds were evaluated. According to Fig. 2a, the live/dead staining results showed that the PLGA/CuBDC@Exo group survived the best and maintained a certain diffusion ability. In addition, the CCK-8 assay was showed in Fig. 2b matched with the cell viability test as well. For PLGA/CuBDC@Exo group, the proliferation rate of hBMSCs was the highest. The osteogenesis and angiogenesis are coupling to each other, the osteogenic and angiogenic protein marker expression after culturing 14 days were evaluated and shown in Fig. 2c. For PLGA/CuBDC@Exo group, the expression of both osteogenic-related proteins (ALP, Runx2, Ocn) and vascular endothelial growth factor (VEGF) showed a distinctly increase, which may be due to the synergistic effect of CuBDC and hBMSCs-Exo in promoting the osteogenic differentiation in hBMSCs to some extent. Besides, VEGF is a pro-angiogenesis factor that facilitates the proliferation, migration and survival of endothelial cells. Thus, it is important for revascularization during osteogenesis, and high expression of VEGF in this scaffold could promote angiogenic activity around endothelial cells, further enhancing the ability of osteogenic regeneration. In addition, the hBMSCs-Exo have been reported to be involved in multiple physiology and pathology activities including osteogenesis, bone regeneration, wound healing and tumorigenesis [38–40], and alleviating bone loss by activating Wnt/β-catenin signaling [41]. Further, we used ALP staining to evaluate osteogenic differentiation and the results were shown in Fig. 2d. Notably, the introduction of hBMSCs-Exo could effectively enhance the osteogenic differentiation ability of the scaffold, and the ARS staining results showed a consistent trend (Fig. 2e). Overall, these results further indicated that the MOF-modified scaffold coated by exosomes had excellent osteogenic properties.

Subsequently, the pro-angiogenic ability of the stents were evaluated. As shown in Fig. S10 (Supporting information), the red-stained exosomes were uniformly distributed in the cytoplasm of HUVECs. It also further illustrated the internalization of exosomes by HUVECS and then performed the corresponding biological functions. More strikingly, the transwell assay (Fig. 2f) and wound-healing assay (Fig. 2g) both revealed that the PLGA/CuBDC@Exo group markedly promoted the migration of HUVECs, while in the PLGA groups only limited cell migration was observed after incubation for 24 h. For then, the tube formation assay was analyzed with the support of matrigel and clarified that compare with other groups, HUVECs treated by PLGA/CuBDC@Exo group formed the maximum number of tube-like and branch-like structures at 6 h (Fig. 2h). Taken together, our results indicated that PLGA/CuBDC@Exo could dramatically enhance *in vitro* angiogenesis of HUVECs.

Benefitting from the *in vitro* results, we further evaluated the osteogenic performance of PLGA/CuBDC@Exo scaffold *in vivo*. At five and ten weeks after implantation, the samples were scanned by Micro-CT (Fig. 3a). The Blank group had only a limited growth; the area of newly formed bone was enlarged in the second group; A bulk mass of new bone was formed in the PLGA/CuBDC@Exo group, which was connected to each other and only a few vacant areas were left after 10 weeks, demonstrating the best osteogenic capability and new bone formation. The statistics analysis further confirmed bone mineral density (BMD) and bone volume/tissue

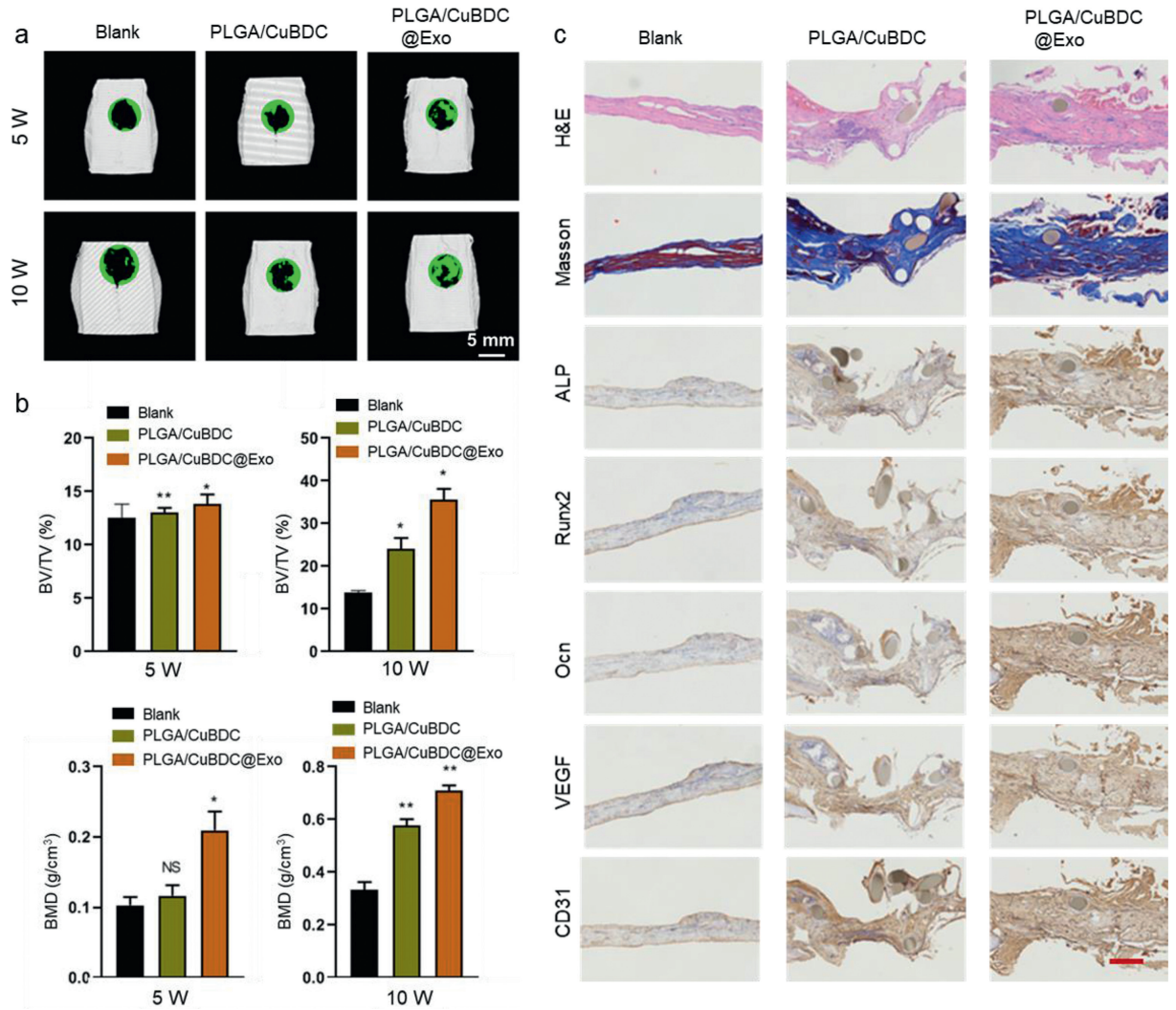

Fig. 3. Representative images of Micro-CT and histological analysis of bone regeneration after 2-month implantation. (a) Micro-CT reconstruction images of defect areas. (b) Quantitative analysis of BV/TV and BMD values in each group. NS, no significance compared to control ($n = 3$), $^{*}P < 0.05$, $^{**}P < 0.01$. (c) Histological evaluation stained with H&E, Masson staining and typical images of immunohistochemistry analysis of ALP, Runx2, Ocn, VEGF and CD31 for new bone formation after 10 weeks (scale bar: 200 μm).

volume (BV/TV) (Fig. 3b). All results indicated the excellent osteoconductive capacity of the PLGA/CuBDC@Exo scaffold *in vivo*. Then, the histological evaluation was performed to visualize new-formed bone tissues in defect areas (Fig. 3c). For PLGA/CuBDC@Exo group, the defect area was covered with bone collagen and more mature osteocytes than the others. Masson staining further verified the above results and more collagen tissue could be seen in the internal space. The immunohistochemical method was proved the activity of bone formation due to the expression of ALP, Runx2, Ocn, VEGF and CD31. The PLGA/CuBDC@Exo scaffold may provide a microenvironment conducive to angiogenesis and stimulate their release from osteoblasts. All results suggested that the composite scaffold could promote vascularized osteogenesis *in vivo*.

To conclude, we fabricated a novel MOF-based fibrous scaffold on which hBMSCs-derived exosomes were immobilized, thereby enabling cell-free therapy for bone defects. The synergy between the MOF-modified scaffolding material and exosomes could dramatically promote the osteogenesis and angiogenesis *in vitro* and powerful bone regeneration *in vivo*. Scaffolds carrying therapeutic exosomes possess good potential application of MOF materials for bone tissue engineering, and further expands the role of exosomes for vascularized osteogenesis.

Declaration of competing interest

The authors declare that they have no known competing financial interests or personal relationships that could have appeared to influence the work reported in this paper.

Acknowledgments

This work was supported by the Fundamental Research Funds for the Central Universities (No. DUT20YG105) and the Joint Foundation of Liaoning Province (No. 2020-ZLLH-40).

Supplementary materials

Supplementary material associated with this article can be found, in the online version, at doi:10.1016/j.cclet.2022.05.042.

References

[1] N.Z. Laird, T.M. Acri, K. Tingle, et al., Adv. Drug Deliv. Rev. 174 (2021) 613–627.
[2] K. Huang, G. Liu, Z. Gu, et al., Chin. Chem. Lett. 31 (2020) 3190–3194.
[3] L. Huang, J. Zhang, X. Liu, et al., Chin. Chem. Lett. 32 (2021) 234–238.
[4] K. Huang, J. Huang, J. Zhao, et al., Chin. Chem. Lett. 31 (2021) 3190–3194.
[5] S. Zhu, S. Bennett, V. Kuek, et al., Theranostics 10 (2020) 5957–5965.

[6] H.A. Rather, D. Jhala, R. Vasita, Mater. Sci. Eng. C 103 (2019) 109761.
[7] H.S. Han, I. Jun, H.K. Seok, et al., Adv. Sci. 7 (2020) 2000800.
[8] C. Xu, Y. Chang, Y. Xu, et al., Adv. Healthc. Mater. 11 (2021) 2101911.
[9] S. Stegen, N. van Gastel, G. Carmeliet, Bone 70 (2015) 19–27.
[10] T. Zhu, M. Jiang, M. Zhang, et al., Bioact. Mater. 9 (2022) 446–460.
[11] F. Diomede, G.D. Marconi, L. Fonticoli, et al., Int. J. Mol. Sci. 21 (2020) 3242.
[12] L. Cui, J. Zhang, J. Zou, et al., Biomaterials 230 (2020) 119617.
[13] A. Mishra, P. Singh, I. Qayoom, et al., J. Mater. Chem. B 9 (2021) 6281–6309.
[14] J. Fan, C.S. Lee, S. Kim, et al., ACS Nano 14 (2020) 11973–11984.
[15] J. Huang, J. Xiong, L. Yang, et al., Nanoscale 13 (2021) 8740–8750.
[16] H.P. Bei, P.M. Hung, H.L. Yeung, et al., Small 17 (2021) 2101741.
[17] M. Zhai, Y. Zhu, M. Yang, et al., Adv. Sci. 7 (2020) 2001334.
[18] Y. Zhang, Y. Xie, Z. Hao, et al., ACS Appl. Mater. Interfaces 13 (2021) 18472–18487.
[19] L. Ding, X. Yang, Z. Gao, et al., Small 17 (2021) 2007174.
[20] L. Xin, X. Lin, F. Zhou, et al., Acta Biomater. 113 (2020) 252–266.
[21] O. Toprak, B. Topuz, Y.A. Monsef, et al., Mater. Sci. Eng. C 120 (2021) 111738.
[22] Y. Xue, Z. Zhu, X. Zhang, et al., Adv. Healthc. Mater. 10 (2021) 2001369.
[23] L. Zhong, J. Chen, Z. Ma, et al., Nanoscale 12 (2020) 24437–24449.
[24] Y. Wang, J. Yan, N. Wen, et al., Biomaterials 230 (2020) 119619.
[25] S. Zhang, X. Pei, H. Gao, et al., Chin. Chem. Lett. 31 (2020) 1060–1070.
[26] J. Zhang, H. Chen, M. Zhao, et al., Nano Res. 13 (2020) 2019–2034.
[27] T. Bai, K. Zhao, Z. Lu, et al., Chin. Chem. Lett. 32 (2021) 1051–1054.
[28] P. Wang, Y. Yuan, K. Xu, et al., Bioact. Mater. 6 (2021) 916–927.
[29] A. El-Fiqi, N. Mandakhbayar, S.B. Jo, et al., Bioact. Mater. 6 (2021) 123–136.
[30] X. Ren, C. Yang, L. Zhang, et al., Nanoscale 11 (2019) 11830–11838.
[31] M. Lian, Y. Han, B. Sun, et al., Acta Biomater 118 (2020) 83–99.
[32] X. Cheng, Z. Zheng, X. Zhou, et al., ACS Sustainable Chem. Eng. 8 (2020) 17783–17790.
[33] X. Cheng, S. Zhang, H. Liu, et al., ACS Appl. Mater. Interfaces 12 (2020) 36996–37005.
[34] D. Zhao, T. Zhu, J. Li, et al., Bioact. Mater. 6 (2021) 346–360.
[35] S. Jin, X. Xia, J. Huang, et al., Acta Biomater. 127 (2021) 56–79.
[36] J. Ding, J. Zhang, J. Li, et al., Prog. Polym. Sci. 90 (2019) 1–34.
[37] X. Gao, S. Han, R. Zhang, et al., J. Mater. Chem. B 7 (2019) 7075–7089.
[38] Q. Zhan, K. Yi, H. Qi, et al., Theranostics 10 (2020) 7889–7905.
[39] M. Wang, C. Wang, M. Chen, et al., ACS Nano 13 (2019) 10279–10293.
[40] Z.W. Luo, F.X.Z. Li, Y.W. Liu, et al., Nanoscale 11 (2019) 20884–20892.
[41] R. Zuo, M. Liu, Y. Wang, et al., Stem Cell Res. Ther. 11 (2020) 33.